A dusty gas flow model in porous media

M.H. HAMDAN

Department of Mathematics and Computer Science, Mount Allison University, Sackville, New Brunswick, Canada E0A 3C0

R.M. BARRON

Department of Mathematics and Statistics, and Fluid Dynamics Research Institute, University of Windsor, Windsor, Ontario, Canada N9B 3P4

Abstract: The differential equations governing the dusty fluid flow in porous media are developed based on Saffman's dusty gas flow equations. The model equations are cast in vorticity-streamfunction forms and applied to study the flow in a rectangular cavity. A numerical solution is obtained for the flow considered and the results are compared with the solution for a clean fluid flow in porous media.

1. Introduction

Fluid flow in porous media is described by the continuity equation together with the momentum equations, which usually take the form of Darcy's law, provided the flow is of the seepage type and the porosity of the medium is sufficiently small.

In cases where the porous medium is not a naturally occurring one, but rather the solid matrix is composed of a loose distribution of solids fixed in space, such as a macromolecular distribution, the porosity might cease to be small enough for Darcy's law to accurately describe the flow phenomena. The momentum equations must take a different form in order to describe the flow more accurately and to account for the relatively high porosity of the medium. One such model is Brinkman's equation, which has proven to be a very important model in describing flow through porous media with high porosities [3].

Many applications of fluid flow through porous media, where Brinkman's model is applicable, were discussed by Wiegel [6]. He considered the flow domain to be composed of a distribution of macromolecules and discussed at length its applications in biophysics. The same model was implemented by Hamdan and Barron [2] in a vorticity-streamfunction formulation to study separated flow in the driven porous cavity.

One of the many important applications of porous media flow is in irrigation problems. In such a case one usually assumes the applicability of Darcy's law in the media considered and single or two-phase flow is usually studied [7]. In cases where the porosity of the medium is high and the flowing fluid contains a small distribution of solid particles we propose a dusty gas flow

model through porous media. Such a model is formulated in terms of Brinkman's equation and is based on Saffman's dusty gas equations. This model has direct applicability to irrigation problems in which the fluid may contain some undissolved solids (fertilizers) or in cases of salty layers of sand undergoing a flushing process.

The flow equations which are developed are cast into vorticity-streamfunction form and applied to study the characteristics of dusty fluid flow in the driven porous cavity model. The structure of the separated corner eddies is also studied to demonstrate the effect of the dust parameters on the flow. Differences between the porous cavity dusty gas flow and the regular cavity dusty gas flow are also indicated.

A numerical approach is taken to accomplish the above study.

2. Model development

The equations governing the flow of an incompressible dusty fluid, in the absence of body forces, can be expressed in the following form [4]:

for fluid-phase:

conservation of mass:

$$\nabla \cdot \boldsymbol{u} = 0; \tag{1}$$

conservation of linear momentum:

$$\rho \left[\frac{\partial \boldsymbol{u}}{\partial t} + (\boldsymbol{u} \cdot \nabla)\boldsymbol{u} \right] = -\nabla p + \mu \nabla^2 \boldsymbol{u} + kn(\boldsymbol{v} - \boldsymbol{u}); \tag{2}$$

for dust-phase:

conservation of mass:

$$\frac{\partial n}{\partial t} + \nabla \cdot (n\boldsymbol{v}) = 0; \tag{3}$$

conservation of linear momentum:

$$mn \left[\frac{\partial \boldsymbol{v}}{\partial t} + (\boldsymbol{v} \cdot \nabla)\boldsymbol{v} \right] = kn(\boldsymbol{u} - \boldsymbol{v}); \tag{4}$$

where $\boldsymbol{u}$ is the fluid-phase microscopic velocity vector, $\boldsymbol{v}$ is the dust-phase microscopic velocity vector, ρ is the fluid density, p is the pressure, μ is the dynamic viscosity, n is the dust particle number density, m is the mass of a single dust particle and k is the Stokes coefficient of resistance.

In order to develop a dusty fluid porous media flow analogy to the above equations we consider Saffman's assumption to be valid for the case of a porous medium. Thus, we assume a very small volume fraction of the dust-phase and consequently zero interaction between the particles. This permits assuming a macroscopic continuum behaviour for the dust particles distribution, and hence we develop a set of equations for the dust-phase and another for the fluid-phase.

Averaging the Navier–Stokes equations using the procedure outlined by Semrau [5] and implementing Saffman's assumptions the following macroscopic governing equations are obtained for each phase:

fluid-phase equations:

$$\nabla \cdot U = 0; \tag{5}$$

$$\rho \left[\frac{\partial U}{\partial t} + (U \cdot \nabla)U \right] = -\nabla P_1 + \mu \nabla^2 U + F_1; \tag{6}$$

where F_1 is the sum of external forces exerted on a unit volume of the fluid-phase, U is the fluid-phase macroscopic velocity vector and P_1 is the macroscopic fluid-phase partial pressure.

The term F_1 is assumed to be comprised of two forces, f_{11} and f_{12}, where f_{11} is the friction force per unit volume of the fluid-phase due to the solid matrix of the porous medium. In order to derive an expression for f_{11} we employ Darcy's law in the form

$$(U - V) = -\frac{\eta}{\mu} \nabla P, \tag{7}$$

where we have assumed that the seepage velocity in Darcy's law is the relative velocity of the fluid- and dust-phases. Accordingly, the friction force f_{11} balances the Darcy's pressure gradient and thus takes the form

$$f_{11} = +\nabla P = -\frac{\mu}{\eta}(U - V), \tag{8}$$

where η is the permeability and V is the macroscopic dust-phase velocity vector. The term f_{12} is the force per unit volume of the fluid-phase due to the influence of dust. Denoting the macroscopic particle number density by N, the assumption of a small concentration of dust, by volume, leads to the following expression for the dust effect on the clean fluid:

$$f_{12} = KN(V - U), \tag{9}$$

where K is the coefficient of resistance in the porous medium, which is constant under the assumption of uniform size and distribution of the dust particles.

For small Reynolds number Re the inertia terms in equation (6) are negligible (cf. [6]) and thus the fluid-phase momentum equations take the following vector form, when equations (8) and (9) are employed in equation (6),

$$-\nabla P_1 + \mu \nabla^2 U + (V - U)\left(KN + \frac{\mu}{\eta}\right) = \rho \frac{\partial U}{\partial t}. \tag{10}$$

dust-phase equations:

The macroscopic dust-phase equations take the form

$$\frac{\partial N}{\partial t} + \nabla \cdot (NV) = 0; \tag{11}$$

$$mN \left[\frac{\partial V}{\partial t} + (V \cdot \nabla)V \right] = F_2, \tag{12}$$

where the force F_2 represents the sum of external forces exerted on a unit volume of the dust. Although it might be possible to consider that F_2 is composed of two forces, one due to the effect of the fluid-phase on the dust-phase while the other is the friction force due to the solid matrix, it is reasonable to assume that the latter force is much smaller than the first due to the assumption of a very small bulk concentration of dust. Furthermore, such small bulk concentration of the dust inhibits the consideration of a separate permeability for the dust-phase and the

relative permeability model is therefore invalid in this context. Thus a separate Darcy's law cannot be considered for the dust-phase.

The saturation in this context will refer only to the fluid, in general, since the idea of miscible and/or immiscible displacement is nonexistent for the type of flow considered.

According to the above the only contributing force is due to the fluid-phase influence on the dust and is given by

$$F_2 = KN(U - V).$$ (13)

Thus the dust-phase momentum equation takes the form

$$mN\left[\frac{\partial V}{\partial t} + (V \cdot \nabla)V\right] = KN(U - V).$$ (14)

As can be seen from equation (14), in this model for the flow of a dusty fluid in porous media, the dust-phase behaviour does not depend directly on the permeability of the medium. It should be noted that the inertia terms in the dust-phase equations are not negligible, for small Re, as in the case of the fluid-phase equations due to the fact that the dust inertia is much larger than that of the fluid-phase.

3. The porous cavity model

The equations developed in the previous section are used to study the dusty fluid motion in a rectangular cavity. Such a motion is assumed to be generated by the steady sliding motion of the top wall of the cavity in its own plane. The cavity walls are assumed to be impermeable while the flow domain is assumed to consist of a porous material.

By considering the steady, rotational, laminar, plane flow of an incompressible viscous dusty fluid, the governing equations reduce to the following:

for dust-phase:

$$\nabla \cdot (NV) = 0;$$ (15)

$$mN(V \cdot \nabla)V = KN(U - V);$$ (16)

for fluid-phase:

$$\nabla \cdot U = 0;$$ (17)

$$-\nabla P_1 + \mu\nabla^2 U + (V - U)\left(\frac{\mu}{\eta} + KN\right) = 0.$$ (18)

Equations (15)–(18) represent a system of six equations in the six unknowns U, V, N and P_1. By taking N to be constant throughout the flow field we notice that the above governing equations render an overdetermined system of six equations and five unknowns. This suggests that the governing dust-phase equations in streamfunction-vorticity form might yield dust-phase velocity components that do not necessarily satisfy equation (16). The dust-phase streamfunction-vorticity formulation is, nevertheless, facilitated by modifying equation (16) to include dust-phase partial pressure P_2 and thus equation (16) is replaced by

$$mN(V \cdot \nabla)V = -\nabla P_2 + KN(U - V).$$ (19)

Using equation (19) and taking N to be constant in equations (15), (18) and (19), the equations of motion are expressed in (nondimensional) streamfunction-vorticity form as:

for dust-phase:

$$\xi_2 = -\frac{\partial^2 \Psi_2}{\partial X^2} - \frac{\partial^2 \Psi_2}{\partial Y^2};$$ (20)

$$\frac{\partial \Psi_2}{\partial Y}\frac{\partial \xi_2}{\partial X} - \frac{\partial \Psi_2}{\partial X}\frac{\partial \xi_2}{\partial Y} = \frac{K}{M}(\xi_1 - \xi_2);$$ (21)

for fluid-phase:

$$\xi_1 = -\frac{\partial^2 \Psi_1}{\partial X^2} - \frac{\partial^2 \Psi_1}{\partial Y^2};$$ (22)

$$\frac{\partial^2 \xi_1}{\partial X^2} + \frac{\partial^2 \xi_1}{\partial Y^2} + \left(KN^*\ \mathrm{Re} + \frac{1}{\eta^*}\right)(\xi_2 - \xi_1) = 0;$$ (23)

where Ψ_1 is the fluid-phase streamfunction, Ψ_2 is the dust-phase streamfunction, ξ_1 is the fluid-phase vorticity, ξ_2 is the dust-phase vorticity, M is the mass of a dust particle, N^* is the number density, X and Y are the dimensionless independent variables, η^* is the dimensionless permeability, $\mathrm{Re} = \rho L V_0/\mu$ is the Reynolds number, V_0 is the moving wall velocity and L is the cavity width.

The governing equations, in streamfunction-vorticity form, were rendered dimensionless with respect to the width of the cavity and with respect to the velocity of the moving wall. The terms K/M and KN/ρ have the dimensions of relaxation time and frequency, respectively. In what follows the asterisk will be dropped from η^* and N^*.

For the type of flow medium considered, it is reasonable to assume that the inertial terms are negligible compared to the dominant viscous terms. In this case the term involving Re in equation (23) vanishes and this equation reduces to

$$\frac{\partial^2 \xi_1}{\partial X^2} + \frac{\partial^2 \xi_1}{\partial Y^2} + \frac{1}{\eta}(\xi_2 - \xi_1) = 0.$$ (24)

By contrast, the equations governing this same type of flow when the flow domain is a regular (nonporous) cavity and Re = 0 take the following streamfunction-vorticity form:

for fluid-phase:

$$\frac{\partial^2 \xi_1}{\partial X^2} + \frac{\partial^2 \xi_1}{\partial Y^2} = 0;$$ (25)

$$\xi_1 = -\frac{\partial^2 \Psi_1}{\partial X^2} - \frac{\partial^2 \Psi_1}{\partial Y^2};$$ (26)

for dust-phase:

$$\frac{\partial \Psi_2}{\partial Y}\frac{\partial \xi_2}{\partial X} - \frac{\partial \xi_2}{\partial Y}\frac{\partial \Psi_2}{\partial X} = \frac{K}{M}(\xi_1 - \xi_2);$$ (27)

$$\xi_2 = -\frac{\partial^2 \Psi_2}{\partial X^2} - \frac{\partial^2 \Psi_2}{\partial Y^2}.$$ (28)

In order to check the validity of the current formulation we expect that when the porosity of the medium approaches unity the porous media dusty fluid flow equations correspond to the regular dusty fluid cavity flow equations at Re = 0 and that when the porosity of the medium becomes small and the velocity is of the seepage type then our governing equations should reduce to Darcy's law.

We notice that, in (24), when the porosity is equal to unity, or equivalently the permeability η becomes infinite, (24) reduces to (25). When the porosity of the medium is small, effectively $\eta \ll 1$, (24) reduces to $\xi_2 - \xi_1 = 0$, which is exactly equation (7) or Darcy's law for the dusty fluid flow considered, with the pressure terms eliminated.

It has been shown [1] that for the dusty fluid flow at Re = 0 in a regular cavity, the fluid-phase vorticity and streamfunction equations are the same as Navier–Stokes equations for the clean fluid flow. It is thus expected that, when $\eta = 1$ in the case of porous media dusty fluid flow, the fluid-phase will behave in a similar manner to the clean fluid flow which in turn behaves like the nonporous media flow at Re = 0. This is due to the fact that all three sets of equations become basically the same when porosity is unity, or equivalently nondimensional permeability is unity.

In terms of the streamfunctions, the dimensionless velocity components are defined by

$$U_1 = \frac{\partial \Psi_1}{\partial Y}, \qquad V_1 = -\frac{\partial \Psi_1}{\partial X}, \qquad U_2 = \frac{\partial \Psi_1}{\partial Y}, \qquad V_2 = -\frac{\partial \Psi_1}{\partial X}.$$

The dimensionless vorticities are defined by

$$\xi_1 = \frac{\partial V_1}{\partial X} - \frac{\partial U_1}{\partial Y} \quad \text{and} \quad \xi_2 = \frac{\partial V_2}{\partial X} - \frac{\partial U_2}{\partial Y}.$$

Once the coupled equations (20)–(22) and (24) are solved for the streamfunction and vorticity of each respective phase, the dust-phase velocity components can be evaluated from the above expressions for U_2 and V_2 in terms of the dust-phase streamfunction. With the knowledge of U_2 and V_2, (19) can then be solved for P_2, which is the dust-phase partial pressure necessary for the computed dust-phase velocity components to satisfy (19) with N taken as a constant.

4. Finite-difference approximations

In order to integrate the governing equations numerically over the chosen flow domain we use the second-order accurate 3-point central differencing scheme to approximate all of the derivatives involved over a uniformly discretized square grid. The difference equations resulting from such approximations are then cast into relations of the form

$$a_{i,j}F_{i,j-1} + b_{i,j}F_{i,j} + c_{i,j}F_{i,j+1} = d_{i,j},$$

where $F_{i,j}$ represents any one of ξ_1, ξ_2, Ψ_1 or Ψ_2 at node (i, j), for $i = 1, 2, \ldots, \text{Imax}$ and $j = 1, 2, \ldots, \text{Jmax}$, and a, b, c, d are coefficients. Such a form is suitable for successive line overrelaxation with sweep along each grid line, $i = 2, 3, \ldots, \text{Imax} - 1$.

The above form of the difference equations produces tridiagonal matrices once (20)–(22) and (24) are expressed for every node (i, j). Diagonal dominance of the resulting tridiagonal matrices is clear for (20), (21) and (24). For (22) diagonal dominance of the resulting matrix is guaranteed provided that the following criterion is met:

$$|hK/M| \geqslant |(V_2)_{i,j}| \quad \text{for } i = 2, 3, \ldots, \text{Imax} - 1 \text{ and } j = 2, 3, \ldots, \text{Jmax} - 1,$$

where h is the step-size.

5. Boundary conditions

Since all of the dependent and independent variables have been rendered dimensionless with respect to the velocity of the moving wall and the width of the cavity, the cavity will be of unit width and of any convenient depth. In this study the depth is taken to be unity and thus we are dealing with a square cavity.

According to the above nondimensionalization, the moving wall has a velocity of magnitude unity. The direction is taken, for convenience, to be in the direction of the negative X-axis so that the streamfunctions obtained will assume positive values.

The only boundary condition used for the fluid-phase is that of no-slip on all of the four cavity walls. Such a condition translates into the following conditions on Ψ_1:

$$\Psi_1 = \frac{\partial \Psi_1}{\partial X} = 0 \text{ for } x = 0, 1 \quad \text{and} \quad 0 \leqslant Y < 1,$$

$$\Psi_1 = \frac{\partial \Psi_1}{\partial Y} = 0 \text{ for } y = 0 \quad \text{and} \quad 0 \leqslant X \leqslant 1,$$

$$\Psi_1 = 0 \quad \text{and} \quad \frac{\partial \Psi_1}{\partial Y} = -1 \text{ for } Y = 1, 0 < X < 1.$$

Since the above conditions do not involve conditions on the fluid-phase vorticity ξ_1, the vorticity boundary conditions are derived by assuming the validity of the flow equations at the boundary and deriving expressions for the fluid-phase vorticity on the four walls in terms of the fluid-phase streamfunction at interior grid points. This of course excludes the top two corners where the vorticity remains undefined due to the difference in velocities on the moving wall and the left and right walls.

Using the image line technique, the following second-order accurate expressions for the fluid-phase vorticity at the walls are obtained:

at the left wall:

$$(\xi_1)_{1,j} = \frac{-2}{\Delta X^2} (\Psi_1)_{2,j} \quad \text{for } j = 1, \dots, \text{Jmax} - 1;$$

at the right wall:

$$(\xi_1)_{\text{Imax},j} = \frac{-2}{\Delta X^2} (\Psi_1)_{\text{Imax}-1,j} \quad \text{for } j = 1, \dots, \text{Jmax} - 1;$$

at the lower wall:

$$(\xi_1)_{i,1} = \frac{-2}{\Delta Y^2} (\Psi_1)_{i,2} \quad \text{for } i = 2, \dots, \text{Imax} - 1;$$

at the moving wall:

$$(\xi_1)_{i,\text{Jmax}} = \frac{-2}{\Delta Y^2} (\Psi_1)_{i,\text{Jmax}-1} + \frac{2}{\Delta Y} \quad \text{for } i = 2, \dots, \text{Imax} - 1.$$

With regard to the dust-phase boundary conditions we note that a no-slip condition on the dust-phase velocity components cannot be imposed in light of the facts that the dust-phase viscous effects are absent and the deposition and collision of some dust particles on the walls

usually causes some other particles to slide off resulting in a slip condition. The assumption of constant number density, however, allows the possibility of assuming zero normal velocity components on the walls, with the nonzero tangential components to be determined.

The assumption of vanishing normal velocity at the four walls of the cavity implies that Ψ_2 is constant on all four walls. For convenience we can choose the walls to constitute the streamline $\Psi_2 = 0$ and thus the dust-phase boundary conditions take the following form:

$$\Psi_2 = -\frac{\partial \Psi_2}{\partial X} = 0 \text{ for } Y = 0, 1 \text{ and } 0 < X < 1;$$

$$\Psi_2 = \frac{\partial \Psi_2}{\partial Y} = 0 \text{ for } X = 0, 1 \text{ and } 0 < Y < 1.$$

The above conditions do not give direct conditions for the dust-phase vorticity on the four walls but vorticity conditions are derived by assuming the validity of the dust-phase flow equations at the boundary and deriving expressions for the vorticity on the four walls in terms of the dust-phase streamfunction at interior grid points. By using second-order accurate forward and backward differencing schemes, together with the fact that $\Psi_2 = 0$ on the walls, the following expressions for the dust-phase vorticity boundary conditions are obtained:

on the lower wall:

$$(\xi_2)_{i,1} = \frac{2(\Psi_2)_{i,2} - (\Psi_2)_{i,3}}{\Delta Y^2} \text{ for } i = 2, \ldots, \text{Imax} - 1;$$

on the upper wall:

$$(\xi_2)_{i,\text{Jmax}} = \frac{2(\Psi_2)_{i,\text{Jmax}-1} - (\Psi_2)_{i,\text{Jmax}-2}}{\Delta Y^2} \text{ for } i = 2, \ldots, \text{Imax} - 1;$$

on the left wall:

$$(\xi_2)_{1,j} = \frac{2(\Psi_2)_{2,j} - (\Psi_2)_{3,j}}{\Delta X^2} \text{ for } j = 2, \ldots, \text{Jmax} - 1;$$

on the right wall:

$$(\xi_2)_{\text{Imax},j} = \frac{2(\Psi_2)_{\text{Imax}-1,j} - (\Psi_2)_{\text{Imax}-2,j}}{\Delta X^2} \text{ for } j = 2, \ldots, \text{Jmax} - 1.$$

6. Solution algorithm

The resulting tridiagonal system is solved using a tridiagonal solver, Thomas' algorithm, with successive line relaxation in the Y-direction. The streamfunction equations have been overrelaxed and the momentum equations underrelaxed.

The solution to the coupled equations together with the pertinent boundary conditions is obtained by implementing the following computational procedure.

For a given permeability η and dust parameters K/M:

Step 1: The flow domain is initialized by giving Ψ_1, Ψ_2, ξ_1 and ξ_2 some small starting values.

Step 2:

2.1: Solve the fluid-phase streamfunction equation, for Ψ_1, using the TRIDIAGONAL solver along each grid line, $i = 2, 3, \ldots, \text{Imax} - 1$. The solution is iterated along each i using SLOR of the form

$$\Psi^{n+1} = \Psi^n + \omega(\Psi_*^{n+1} - \Psi^n),$$

where Ψ_*^{n+1} is the value obtained by the TRIDIAGONAL solver, and Ψ^n is the value obtained from the previous iteration.

2.2: Step 2.1 is repeated five times in order to accelerate convergence.

Step 3: Solve the dust-phase streamfunction equation, for Ψ_2, using the method of Step 2.

Step 4: The values of ξ_1 and ξ_2 are calculated at the four walls (excluding the top two cavity corners) using expressions discussed in Section 5 for the vorticities at the walls.

Step 5: Solve the fluid-phase vorticity equation, for ξ_1, by a similar method to that in Step 2.

Step 6: Solve the dust-phase vorticity equation, for ξ_2, using the method of Step 2.

Step 7: Repeat Steps 2–6 until the following convergence criterion is met:

$$\left| F_{i,j}^{n+1} - F_{i,j}^n \right| < \epsilon,$$

where ϵ is the error tolerance, taken as $5 \cdot 10^{-5}$.

Step 8: The velocity components U_1, V_1, U_2 and V_2 are calculated in the flow field using second-order accurate central differencing of their respective definitions in terms of Ψ_1 and Ψ_2.

Step 9: The velocity component U_2 is then calculated on the lower and upper walls and V_2 is calculated on the right and left walls using the following second-order accurate upwind differencing schemes:

on the lower wall:

$$(U_2)_{i,1} = \frac{4(\Psi_2)_{i,2} - (\Psi_2)_{i,3}}{2\,\Delta Y};$$

on the upper wall:

$$(U_2)_{i,\text{Jmax}} = \frac{(\Psi_2)_{i,\text{Jmax}-2} - 4(\Psi_2)_{i,\text{Jmax}-1}}{2\,\Delta Y};$$

on the left wall:

$$(V_2)_{1,j} = \frac{4(\Psi_2)_{2,j} - (\Psi_2)_{3,j}}{2\,\Delta X};$$

on the right wall:

$$(V_2)_{\text{Imax},j} = \frac{(\Psi_2)_{\text{Imax}-2,j} - 4(\Psi_2)_{\text{Imax}-1,j}}{2\,\Delta X}.$$

In the above algorithm the error check is made at all grid points (i, j) if $F_{i,j}$ stands for vorticities and is made at all interior grid points if $F_{i,j}$ stands for the streamfunctions. Solutions using the above algorithm were obtained for the range of dust parameters $K/M = 5$, 10 and 20 and for permeability values $\eta = 0.1$, 0.01 and 0.001 and also for Re = 0. The step-size used is $h = \Delta X = \Delta Y = 0.05$, which corresponds to a 21 × 21 grid.

It should be noted that the obtained solutions satisfied both of the continuity equations to within a maximum error of 10^{-6}.

7. Results and discussion

7.1. Moving wall vorticities

Table 1 shows the values of dust-phase vorticity at the moving wall of the cavity for different characteristic permeability values and different dust parameters. The comparison is also made with the dust-phase vorticity when Re = 0.

For all of the cases considered Table 1 demonstrates that the minimum vorticity occurs at $X = 0.95$ on the moving wall. The maximum value of vorticity occurs at $X = 0.1$ when Re = 0 and at $X = 0.85$ when $K/M = 10$ and $\eta = 0.1$ and 0.01. A further decrease in permeability, when $K/M = 10$, results in shifting the location of the maximum vorticity towards the downstream direction on the upper wall, as can be seen when $\eta = 0.001$ the maximum vorticity value occurs at $X = 0.8$. The nonuniform increase and decrease in the moving wall dust-phase vorticity occurs near the upstream and downstream corners on the moving wall.

For a given characteristic permeability and different dust parameters Table 1 also shows the dust-phase vorticity values at the moving wall for $\eta = 0.01$ and $K/M = 5$, 10 and 20. The minimum value of vorticity for all of these cases occurs at $X = 0.95$. The maximum value occurs at $X = 0.85$ for $K/M = 20$ and 10 and with a further reduction of K/M the location of maximum vorticity occurs further downstream, at $X = 0.8$ when $K/M = 5$.

In Table 2 the fluid-phase vorticity values at the moving wall are illustrated for different permeability values and different dust parameters. The data demonstrates the symmetric vortic-

Table 1
Dust-phase vorticity at the moving wall for different flow parameters

X	$K/M = 10$				$\eta = 0.01$	
	Re = 0	$\eta = 0.1$	$\eta = 0.01$	$\eta = 0.001$	$K/M = 5$	$K/M = 20$
0.05	6.3368	6.3248	6.2155	5.3178	5.4270	6.2818
0.10	7.9173	7.8940	7.6893	6.3433	6.5766	8.2463
0.15	7.5419	7.5166	7.3026	6.2136	6.5245	7.9190
0.20	6.9369	6.9144	6.7303	6.0281	6.2004	7.2096
0.25	6.3439	6.3259	6.1861	5.8968	6.9331	6.5345
0.30	5.9234	5.9110	5.8227	5.9124	5.7645	6.0242
0.35	5.6430	5.6361	5.5985	6.0108	5.7071	5.6777
0.40	5.5056	5.5042	5.5158	6.1993	5.7382	5.4793
0.45	5.4877	5.4916	5.5478	6.4399	5.8481	5.4124
0.50	5.5848	5.5934	5.6887	6.7301	6.0201	5.4673
0.55	5.7884	5.8008	5.9271	7.0494	6.2449	5.6406
0.60	6.0950	6.1102	6.2572	7.3900	6.5084	5.9336
0.65	6.4956	6.5122	6.6670	7.7336	6.7954	6.3478
0.70	6.9695	6.9857	7.1335	8.0575	7.0791	6.8769
0.75	7.4652	7.4792	7.6046	8.3158	7.3114	7.4861
0.80	7.8648	7.8751	7.9656	8.4168	7.3978	8.0684
0.85	7.9143	7.9202	7.9713	8.1629	7.1492	8.3511
0.90	7.1136	7.1159	7.1353	7.1432	6.2033	7.7354
0.95	4.6771	4.6776	4.6820	4.6423	3.9965	5.1972

Table 2
Fluid-phase vorticity at the moving wall for different flow parameters

| X | K/M = 10 | | | | η = 0.01 | |
	Re = 0	η = 0.1	η = 0.01	η = 0.001	K/M = 5	K/M = 20
0.05	29.921	28.894	28.657	27.077	28.563	28.769
0.10	19.792	19.752	19.408	17.559	19.272	19.557
0.15	14.186	14.147	13.821	12.362	13.658	13.962
0.20	10.863	10.829	10.551	9.509	10.396	10.676
0.25	8.839	8.812	8.590	7.978	8.484	8.694
0.30	7.564	7.543	7.375	7.188	7.297	7.456
0.35	6.750	6.734	6.617	6.899	6.601	6.673
0.40	6.243	6.233	6.167	6.953	6.224	6.195
0.45	5.965	5.960	5.948	7.276	6.087	5.944
0.50	5.876	5.878	5.925	7.814	6.149	5.883
0.55	5.965	5.974	6.089	8.544	6.399	6.003
0.60	6.243	6.260	6.452	9.459	6.844	6.318
0.65	6.750	6.777	7.054	10.574	7.517	6.867
0.70	7.564	7.602	7.970	11.933	8.487	7.732
0.75	8.839	8.888	9.345	13.627	9.886	9.061
0.80	10.863	10.921	11.445	15.834	11.970	11.136
0.85	14.186	14.247	14.785	18.908	15.238	14.488
0.90	19.792	19.843	20.292	23.534	20.610	20.061
0.95	29.921	28.947	29.173	30.772	29.309	29.065

ity values for Re = 0 and the loss of such symmetry when the dust is introduced. The minimum value of fluid-phase vorticity is seen to occur at $X = 0.5$ for the cases of $K/M = 10$ and Re = 0, $\eta = 0.1$ and $\eta = 0.01$. When the permeability is reduced to 0.001 the minimum vorticity occurs at $X = 0.35$. The maximum vorticity values occur at $X = 0.95$ for all cases considered, except at Re = 0 where the maximum occurs at $X = 0.05$ and $X = 0.95$.

When $\eta = 0.01$ Table 2 also demonstrates the fluid-phase vorticity at the moving wall for different K/M and shows that while minimum vorticity occurs at $X = 0.5$ when $\eta = 0.01$ and $K/M = 10$ and $K/M = 20$, this minimum occurs at $X = 0.45$ when $K/M = 5$. By contrast with the dust-phase vorticity at the moving wall, fluid-phase vorticity varies more uniformly. This behaviour indicates that the dust-phase does not have much influence on the fluid-phase vorticity at the moving wall for the type of the porous medium considered.

7.2. Velocity profiles

As explained earlier, the velocity boundary condition employed for the fluid-phase is that of no-slip at all solid walls but the condition of vanishing normal components of velocity at all four walls was employed for the dust-phase. This latter condition is a consequence of assuming a constant number density for the dust-phase and thus the dust particles are assumed to reflect off the walls. Of course, this leaves the tangential components of dust-phase velocity to be determined.

In Fig. 1 the dust-phase tangential velocity component at the moving wall is illustrated for different dust parameters and permeability $\eta = 0.01$. The figure shows that the velocity curves
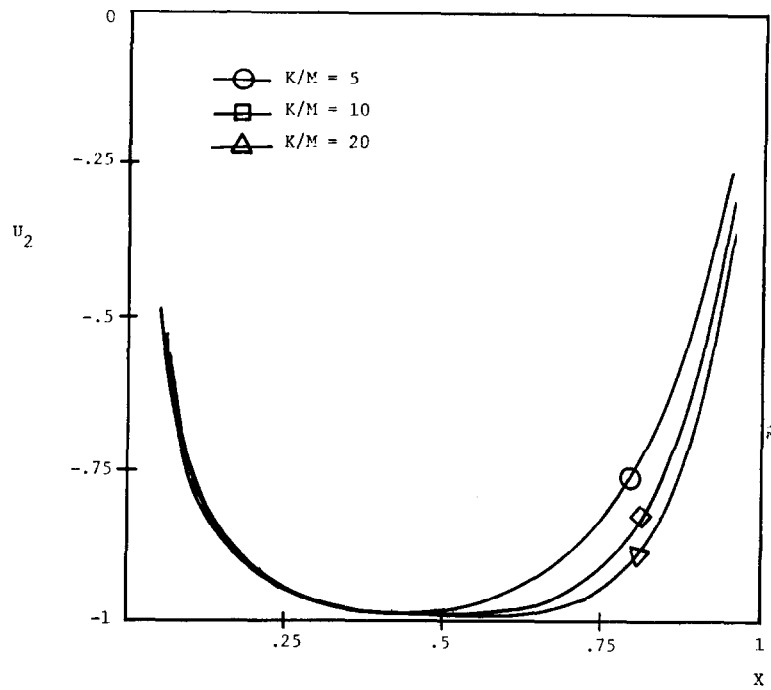
Fig. 1. U_2-velocity component along the moving wall for different K/M, $\eta = 0.01$.
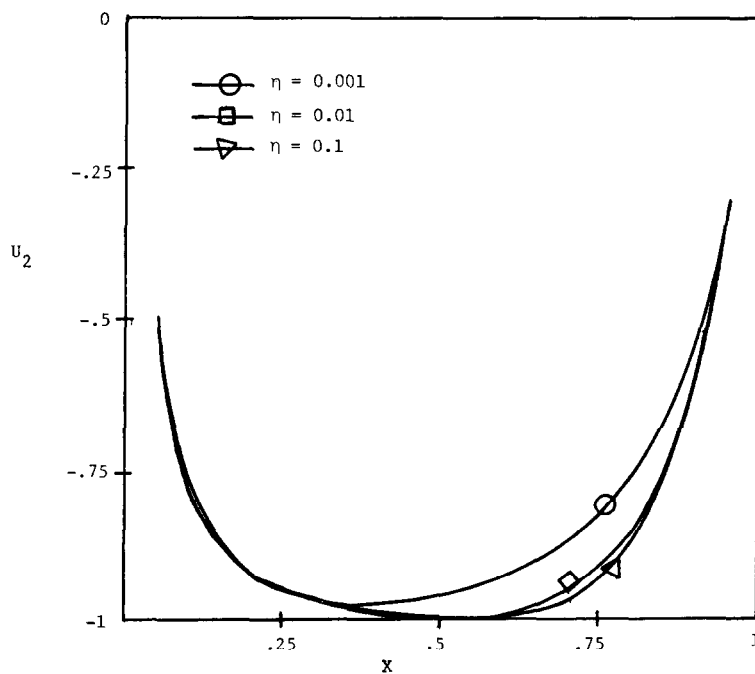

Fig. 2. U_2-velocity component at the moving wall for different permeabilities, $K/M = 10$.
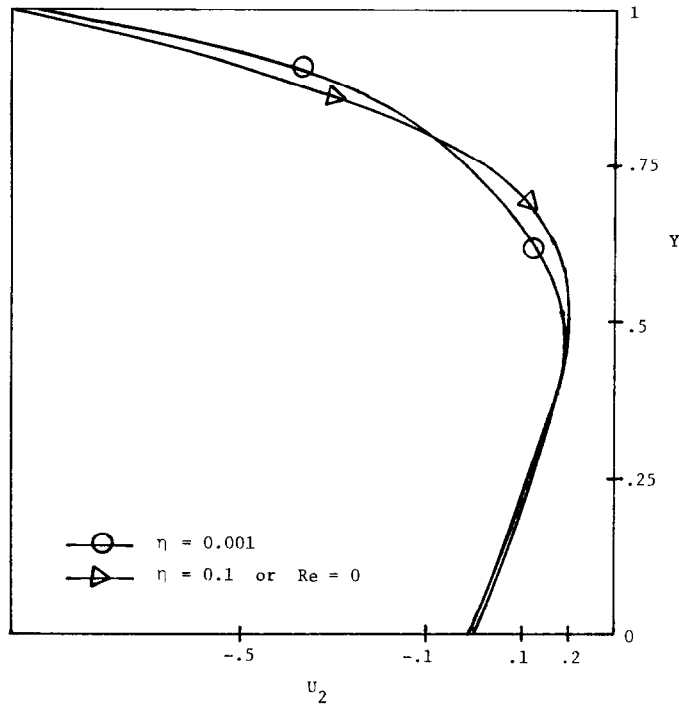
Fig. 3. U_2-velocity component along the vertical centreline for different permeabilities, $K/M = 10$.

are close to each other in the downstream half of the moving wall while the velocity increases, in absolute value, with increasing K/M in the upstream half of the moving wall. For $K/M = 10$ and different permeability values Fig. 2 illustrates the dust-phase tangential component of velocity at the moving wall and demonstrates the reduction of this component with decreasing permeability.

In Fig. 3 the dust-phase horizontal component of velocity at the vertical centreline of the cavity is illustrated for $K/M = 10$ and different permeability values and it shows that the profiles are very close to each other when $Re = 0$ and $\eta = 0.1$. When $\eta = 0.001$, a difference in the velocity occurs and the dust-phase horizontal component of velocity is slightly larger than that when $Re = 0$ in the interval $0 < Y < 0.45$ and is smaller in the interval $0.45 < Y \leqslant 1$.

The fluid-phase horizontal component of velocity along the vertical centreline of the cavity is illustrated in Fig. 4 which demonstrates the velocity for $\eta = 0.001$ when $K/M = 10$ and compares it with the velocity for $\eta = 0.1$. The figure shows that such velocity is slower in the first case than in the second in the interval $0.45 < Y \leqslant 1$ and is slightly faster in the interval $0 < Y < 0.45$.

Although the effect of dust on the fluid-phase horizontal component of velocity along the vertical centreline is hardly noticible, the dust effect is more accentuated when the vertical fluid-phase velocity component along the horizontal centreline of the cavity is considered. Figure 5 illustrates this velocity component for $\eta = 0.001$ and $K/M = 10$, $\eta = 0.01$ and $K/M = 5$ and 20 and demonstrates that when $\eta = 0.001$ and $K/M = 10$ this velocity component is larger, in absolute value, than that for the other cases in the interval $0 < X < 0.3$ and is smaller, in absolute
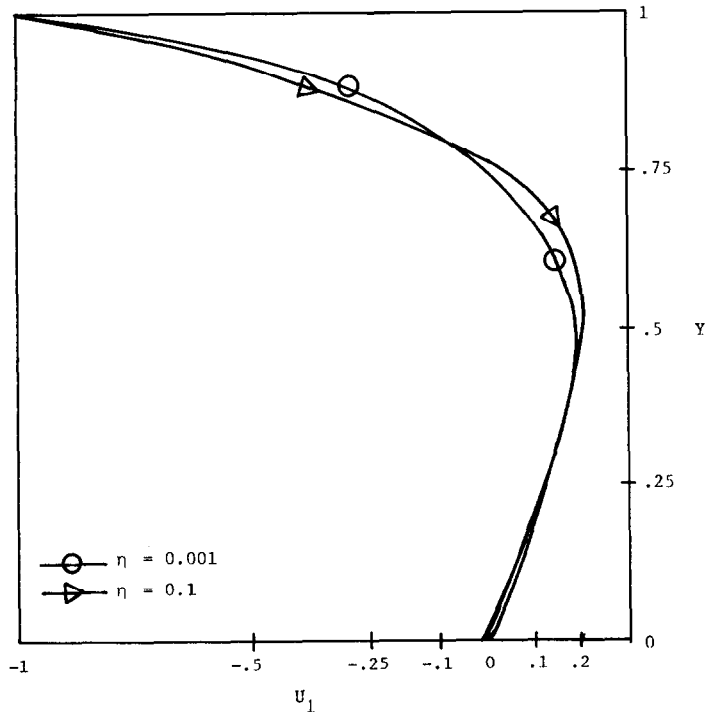
Fig. 4. U_1-velocity component along the vertical centreline for different permeabilities, $K/M = 10$.
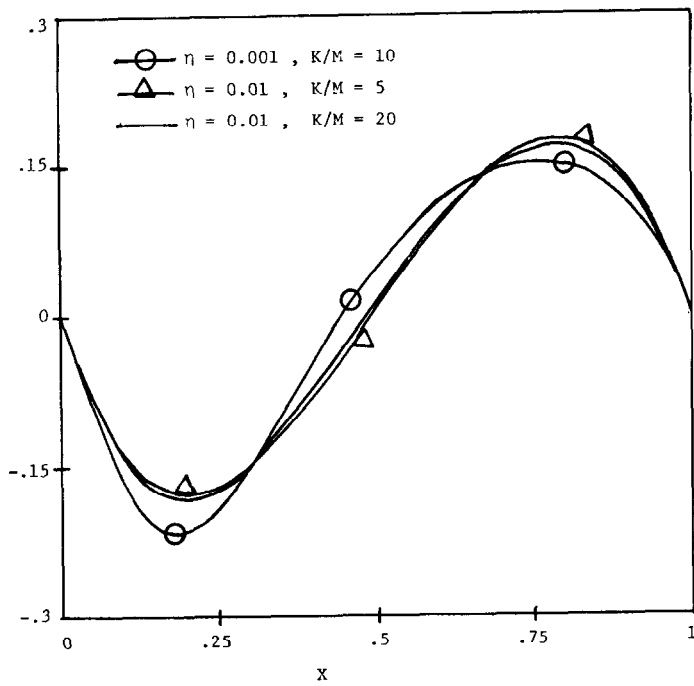

Fig. 5. V_1-velocity component along the horizontal centreline for different permeabilities.

value, than that for the other cases in the interval $0.3 < X < 1$. Figure 5 also shows the effect of increasing and decreasing K/M, for $\eta = 0.01$, on the vertical velocity component.

7.3. Vortex centre location

Table 3 illustrates the magnitudes of the largest fluid-phase streamfunction for all of the cases considered. It also gives the comparison with the dust-phase streamfunction magnitude at the same locations. When $K/M = 10$ the streamfunctions of highest values are largest for $Re = 0$. As permeability is decreased, the streamfunction values decrease at the fluid-phase vortex centres. The location of each of these vortex centres is at $(X, Y) = (0.5, 0.75)$ except in the case of $\eta = 0.001$ when the vortex centre occurs at $(X, Y) = (0.4, 0.75)$. For $\eta = 0.01$ and different K/M, Table 3 demonstrates the increase in the vortex centre streamfunction values, for both of the phases present, with increasing K/M. For $\eta = 0.01$, the location of the vortex centre is, once again, at $(X, Y) = (0.5, 0.75)$ except when $K/M = 5$, when the centre is at $(X, Y) = (0.45, 0.75)$.
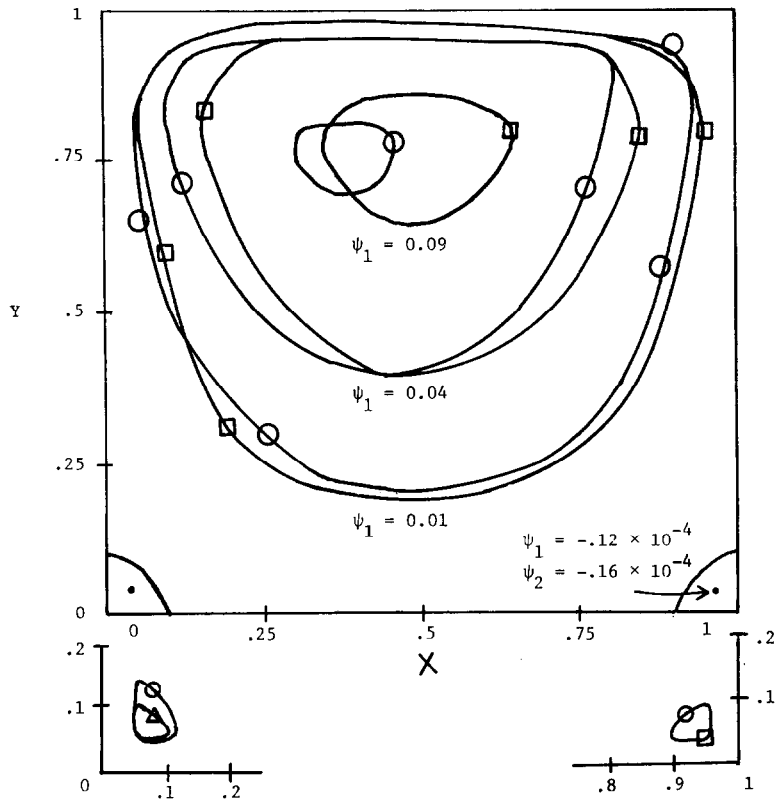
7.4. Flow development

The flow development for $K/M = 10$ and different permeability values is shown in Fig. 6. This figure illustrates the fluid-phase streamlines $\Psi_1 = 0.09$, 0.04 and 0.01 for $K/M = 10$ and $\eta = 0.1$ and 0.001.

When $\eta = 0.1$ the streamlines are very close to the streamlines at $Re = 0$ and thus are not shown here. For a given K/M the streamline $\Psi_1 = 0.09$ spans a smaller area when the permeability is reduced from 0.1 to 0.001. A shift in this streamline, towards the downstream of the upper part of the cavity, also takes place. Such a shift is also noted for the streamlines $\Psi_1 = 0.04$ and 0.01, except that it is less severe than the shift in $\Psi_1 = 0.09$. The area spanned by the streamline $\Psi_1 = 0.04$ is almost the same for both permeabilities considered.

For a given permeability and different dust parameters the streamlines remain close to each other, indicating the minimal effect that the dust-phase has on these streamlines. This fact was also seen when discussing the velocity profiles.

Table 3
Streamfunctions at the fluid-phase vortex centres

	K/M	5	10	20
$Re = 0$	Ψ_1		0.099235	
	Ψ_2		0.098674	
$\eta = 0.1$	Ψ_1		0.099206	
	Ψ_2		0.098622	
$\eta = 0.01$	Ψ_1	0.097183	0.098545	0.099073
	Ψ_2	0.096284	0.097743	0.098872
$\eta = 0.001$	Ψ_1		0.094327	
	Ψ_2		0.094033	

Fig. 6. Primary and secondary streamlines.

7.5. Secondary eddies

For the case of clean fluid flow in a porous rectangular cavity, secondary corner eddies developed for all values of permeability [3]. The secondary eddy with largest streamfunction value occurred when $\eta = 1$ with fluid streamfunction value of $-0.12 \cdot 10^{-4}$. A reduction in the permeability resulted in a reduction of the streamfunction value of the secondary eddy. For $\eta = 0.5$ it took the value $-0.11 \cdot 10^{-4}$ while for $\eta = 0.1$ the maximum streamfunction of the

secondary eddy was found to be $-0.67 \cdot 10^{-5}$. These values were the same for both the upstream and downstream eddies and both of these eddies retained the same dimensions.

As dust is introduced to the fluid it is found that when $K/M = 10$ the secondary eddies have the same dimensions both upstream and downstream for both of the phases present, provided that $\eta \geqslant 0.01$. The largest streamfunction values are, nevertheless, different for each phase. For Re = 0 the largest fluid-phase streamfunction value in the secondary eddy is $\Psi_1 = -0.12 \cdot 10^{-4}$, both upstream and downstream, and this value is the same for $\eta = 0.1$ and 0.01. The dust-phase streamfunction has the value $\Psi_2 = -0.16 \cdot 10^{-4}$ in the downstream corner, while it has the value $-0.18 \cdot 10^{-4}$ in the upstream corner, when Re = 0, and these values remain the same for $\eta = 0.1$ and 0.01.

When K/M is increased from 10 to 20 it is noticed that the fluid-phase secondary eddies have the same values as those when Re = 0 but the dust-phase streamfunction values in the secondary eddies are different, the upstream one taking the value $-0.14 \cdot 10^{-4}$ while the downstream one has the value $-0.13 \cdot 10^{-4}$.

For the cases of $K/M = 5$ and $\eta = 0.01$, and $K/M = 10$ and $\eta = 0.001$, Fig. 6 also demonstrates the relative sizes of the secondary eddies of the two phases involved.

References

[1] R.M. Barron and M.H. Hamdan, The structure of separated dusty gas flow at low and moderate Re, *Internat. J. Engrg. Sci.* **27** (3) (1989) 261–275.

[2] M.H. Hamdan and R.M. Barron, Shear-driven flow in a porous cavity, *J. Fluids Engrg. ASME Trans.* **111** (1989) 433–438.

[3] J. Rubinstein, Effective equations for flow in porous media with a large number of scales, *J. Fluid Mech.* **170** (1986) 379–383.

[4] P.G. Saffman, On the stability of laminar flow of a dusty gas, *J. Fluid Mech.* **13** (1) (1962) 120–128.

[5] J.T. Semrau, Analysis of two phase flow through low-permeability media, Ph.D. Thesis, School of Advanced Studies of Illinois Institute of Technology, Chicago, IL, 1986.

[6] F.W. Wiegel, *Fluid Flow Through Porous Macromolecular Systems*, Lecture Notes in Phys. **121** (Springer, Berlin, 1980).

[7] C.H. Yih, *Dynamics of Nonhomogeneous Fluids* (Macmillan, New York, 1965).